sciendo

TATRA MOUNTAINS
Mathematical Publications

DOI: 10.2478/tmmp-2025-0016
Tatra Mt. Math. Publ. ?? (2025), 1–24

GLOBAL GRAVITY FIELD MODELLING BY SOLVING THE INFINITE NONLINEAR FIXED GEODETIC BOUNDARY VALUE PROBLEM

Marek Macák — Zuzana Minarechová — Róbert Čunderlík — Karol Mikula

Faculty of Civil Engineering, Slovak University of Technology, Bratislava, SLOVAKIA

ABSTRACT. The aim of presented paper is to solve the nonlinear geodetic boundary value problem (BVP) by the finite element method (FEM) involving the mapped infinite elements (MIE). In comparison to our previous works, see [Macák, M. et al.: *On an iterative approach to solving the nonlinear satellite-fixed geodetic boundary-value problem.* In: IAG Symp. Vol. 142 (2016), pp. 185–192.] and [Macák, M. et al.: *A gravity field modelling in mountainous areas by solving the nonlinear satellite-fixed geodetic boundary value problem with the finite element method*, Acta Geodaetica et Geophysica, **58** (2023), 305–320.] dealing with bounded domains, in this paper we propose and study numerical concept on unbounded domains, given as an exterior BVP for the Laplace equation outside the gravitating body, e.g. Earth, with the nonlinear boundary condition (BC) prescribed on the Earth's surface and considering the solution regularity condition at infinity. This concept can be found in many scientific disciplines being also the most natural from physical geodesy point of view, see, e.g., [Backus, G. E.: *Application of a non-linear boundary-value problem for Laplace's equation to gravity and geomagnetic intensity surveys*, Q. J. Mech. Appl. Math. **2** (1968), 195–221.] and of large practical importance when we are not able to prescribe BCs on a bounded domain. The proposed concept is based on the iterative procedure, and as the numerical method we have implemented the FEM with the MIE to take into account the regularity of the disturbing potential at infinity. Since the boundary of the computational domain is the discretized real Earth's surface considering its topography, as finite and infinite elements we have chosen the triangular prisms. We study and verify this numerical approach by a testing experiment with a homogeneous sphere, by the experiment using EGM2008, and finally, we present one detailed numerical experiment with DTU21GRA data.

2020 Mathematics Subject Classification: 35J25,65N30.
Keywords: Fixed geodetic boundary value problem, nonlinear boundary condition, iterative procedure, finite element method, mapped infinite element, global gravity field modelling.
Supported by the Grants APVV-23-0186 and VEGA 1/0690/24.

1. Introduction

From publishing the fundamental studies of physical geodesy written by Stokes [33] and later by Molodensky et al. [25], a determination of the external gravity field has been performed by solving the geodetic boundary value problems (GBVPs). There are various kinds of GBVPs depending on input data and the knowledge of the 3D position of the Earth's surface. In the past, when the vertical information of the Earth's surface was based on levelling, the free GBVPs with gravity anomalies as input data have been solved in practical solutions. Even nowadays, the free GBVP is still solved for local gravity field modelling (e.g., [9]). However, thanks to the precise 3D positioning by GNSS (Global Navigation Satellite Systems) techniques, the absolute 3D position of the Earth's surface is known, so the fixed GBVP is increasingly becoming a subject of interest. Hence, the fixed BVP is reduced to the determination of the geopotential $W(x, y, z)$ in the external space outside the Earth with the gravity measurements observed on the Earth's surface as boundary conditions (BC). It is worth mentioning that there are plenty of approaches and methods routinely used for gravity field modelling. Therefore, here we only mention those that are focused on the fixed GBVP and preferably its original nonlinear form.

The first studies on the theory of the fixed GBVP have been formulated by Backus [2] and Hotine [16]. Few years later, Koch and Pope [18] presented the proof of uniqueness and existence for the nonlinear fixed GBVP, and Bjerhammar and Svensson [7] used the general implicit function theorem to give a solution of the existence and uniqueness problem. The study presenting an expansion of the nonlinear BC into a Taylor series using the reference potential field approximating the geopotential was published by Heck [13] and this approach was later extended by Heck and Seitz [14]. Sacerdote and Sansó [30] published the study where they further developed the idea used by Bjerhammar and Svensson [7] for an iterative solution and they found explicit convergence conditions. Diaz et al. [10,11] showed the existence and uniqueness of a viscosity solution for the Backus problem.

In general, in physical geodesy the most preferred mathematical parametrisation of the gravitational potential is spherical harmonic expansion outside the minimum Brillouin sphere, see, e.g., [27]. There are two reasons for that. The first one is that constant spherical harmonic coefficients defining physical properties of the gravitating body can be estimated by forward modelling or from available gravitational datasets. Second, having a set of the constant spherical harmonic coefficients at disposal, one can simply synthesise the gravitational potential and its higher-order spatial derivatives anywhere in the three-dimensional space, see [37]. There many scientists and researchers who are working on this

issue and the problems connected with it, but since we are dealing with numerical methods in this paper, we recommend readers who are interested in this topic, e.g., [3, 17, 26, 32, 35–37] and the references therein.

Macák et al. [19] published a numerical approach for solving the nonlinear satellite-fixed GBVP by the finite volume method, and recently also by the finite element method (FEM) [22]. In both papers, the infinite computational domain was truncated by adding an artificial boundary away from the Earth, and the numerical solutions have been fixed by the prescribed Dirichlet BC in terms of the disturbing potential. In this paper, we continue in our previous studies [19, 22], but we solve the original infinite nonlinear fixed geodetic boundary value problem (INFGBVP) including the condition of the regularity at infinity. The main motivation of this contribution is the global gravity field modelling in the case when only gravity disturbances on the Earth's surface are available. As a numerical method we have implemented the FEM with mapped infinite elements (MIE), see, e.g., Bettess [5, 6], Zienkiewicz et al. [38, 39] or Macák et al. [21]. An advantage of using numerical methods for solving the fixed GBVP is that numerical solutions can be obtained on the discretized real Earth's surface considering its topography. This can be challenging in high-mountainous areas where a contribution of the nonlinearity is expected to be significant.

The paper is organized as follows. In Section 2, we formulate the INFGBVP with its form for iterative approach. In Section 3, we derive a numerical scheme for solving the infinite fixed GBVP with the oblique derivative BC by the FEM with MIE. Numerical experiments are presented in Section 4. The paper ends with conclusion and summary.

2. Formulation of the infinite nonlinear fixed geodetic boundary value problem and the iterative procedure

Let us consider the infinite computational domain Ω in the space above the Earth, that is, the domain bounded by $\partial\Omega$ representing the Earth's surface and extending to infinity. In such a domain Ω, we formulate the nonlinear infinite fixed geodetic boundary value problem in the following form

$$\Delta T(\mathbf{x}) = 0, \qquad \mathbf{x} \in \Omega, \tag{1}$$

$$\big|\nabla\big(T(\mathbf{x}) + U(\mathbf{x})\big)\big| = g\big(\mathbf{x}\big), \quad \mathbf{x} \in \partial\Omega, \tag{2}$$

$$T(\mathbf{x}) = 0, \qquad |\mathbf{x}| \to \infty, \tag{3}$$

where $T(\mathbf{x})$ is the disturbing potential defined as a difference between the real $W(\mathbf{x})$ and normal $U(\mathbf{x})$ gravity potential generated by a reference ellipsoid GRS80 [15] at any point $\mathbf{x} = (x, y, z)$, $g(\mathbf{x})$ the magnitude of total gravity vector, $\partial\Omega$ is the surface of Earth or more generally any Lipschitz boundary, and $T(\mathbf{x})$ is regular at infinity.

Eqs. (1)–(3) represent an exterior BVPfor the Laplace equation, where the infinite computational domain lies outside the Earth and the equation (2) represents the nonlinear BC. From mathematical point of view, the equation (2) is the so-called eikonal equation that is a nonlinear partial differential equation encountered, e.g., in problems of wave propagation, see [31].

The iterative procedure for determining the direction of $g(\mathbf{x})$ and the disturbing potential $T(\mathbf{x})$ in solving the nonlinear satellite-fixed GBVP has been published in [19] or [22]. Now we will apply its main ideas also for solving INFGBVP.

The norm of the gradient in (2) can be rewritten in the following form

$$\frac{\nabla(T(\mathbf{x})+U(\mathbf{x}))}{|\nabla(T(\mathbf{x})+U(\mathbf{x}))|}\cdot\nabla\big(T(\mathbf{x})+U(\mathbf{x})\big)=g(\mathbf{x}). \tag{4}$$

If we denote the unit vector that defines the direction of the gravity vector, i.e., $\frac{\nabla(T(\mathbf{x})+U(\mathbf{x}))}{|\nabla(T(\mathbf{x})+U(\mathbf{x}))|}=\frac{\nabla(W(\mathbf{x}))}{|\nabla(W(\mathbf{x}))|}$, by $\mathbf{v}(\mathbf{x})$, after some rearrangement in (4) we obtain the equation, which will form the basis of our iterative procedure

$$\mathbf{v}(\mathbf{x})\cdot\nabla\big(T(\mathbf{x})\big)=g(\mathbf{x})-\mathbf{v}(\mathbf{x})\cdot\nabla\big(U(\mathbf{x})\big),\qquad \mathbf{x}\in\partial\Omega. \tag{5}$$

Now we are able to write the iterative procedure for solving INFGBVP as follows

$$\Delta T^{n+1}(\mathbf{x})=0, \qquad \mathbf{x}\in\Omega, \tag{6}$$

$$\mathbf{v}^n(\mathbf{x})\cdot\nabla\big(T^{n+1}(\mathbf{x})\big)=g(\mathbf{x})-\mathbf{v}^n(\mathbf{x})\cdot\nabla\big(U(\mathbf{x})\big), \quad \mathbf{x}\in\partial\Omega, \tag{7}$$

$$T^{n+1}(\mathbf{x})=0, \qquad |\mathbf{x}|\to\infty, \tag{8}$$

for $n=0,1,2,\ldots$, where

$$\mathbf{v}^n(\mathbf{x})=\frac{\nabla(T^n(\mathbf{x})+U(\mathbf{x}))}{|\nabla(T^n(\mathbf{x})+U(\mathbf{x}))|}. \tag{9}$$

We start the iterations with $T^0(\mathbf{x})=0$, so for $\mathbf{v}^0(\mathbf{x})$ we obtain $\mathbf{v}^0(\mathbf{x})=\frac{\nabla(U(\mathbf{x}))}{|\nabla(U(\mathbf{x}))|}=\mathbf{s}(\mathbf{x})$, where $\mathbf{s}(\mathbf{x})$ represents the direction of the normal gravity vector. In this way, in every iteration we solve the BVP for $T^{n+1}(\mathbf{x})$ with the prescribed oblique derivative vector $\mathbf{v}^n(\mathbf{x})$, while in the first one it is given by

$$\mathbf{s}(\mathbf{x})\cdot\nabla\big(T^1(\mathbf{x})\big)=g(\mathbf{x})-\gamma(\mathbf{x})=\delta g(\mathbf{x}), \tag{10}$$

where $\gamma(\mathbf{x})=\big|\nabla\big(U(\mathbf{x})\big)\big|$ denotes a magnitude of the normal gravity vector and $\delta g(\mathbf{x})$ stands for the gravity disturbance.

It means that in each step of our iterative process (6)–(8) we will deal with the infinite fixed GBVP with the oblique derivative BC defined as

$$\Delta T(\mathbf{x})=0, \qquad \mathbf{x}\in\Omega, \tag{11}$$

$$\mathbf{v}(\mathbf{x})\cdot\nabla\big(T(\mathbf{x})\big)=g(\mathbf{x})-\mathbf{v}(\mathbf{x})\cdot\nabla\big(U(\mathbf{x})\big)=\alpha(\mathbf{x}), \quad \mathbf{x}\in\Gamma, \tag{12}$$

$$T(\mathbf{x})=0, \qquad |\mathbf{x}|\to\infty, \tag{13}$$

During the iterative process we improve the direction of the unit vector $\mathbf{v}(\mathbf{x})$ and we stop the computations, if in each node holds

$$|T^n(\mathbf{x}) - T^{n+1}(\mathbf{x})| < \varepsilon, \tag{14}$$

where ε is a user-specified small real number.

Since the last iteration represents the approximation of the disturbing potential $T(\mathbf{x})$ and direction of gravity vector $\mathbf{v}(\mathbf{x})$ in (1)–(3), the sum $T^{n+1}(\mathbf{x})+U(\mathbf{x})$ represents the approximation of the gravity potential $W^{n+1}(\mathbf{x})$ in every node of the computational domain Ω.

3. Solution to the infinite fixed GBVP with the oblique derivative BC by the FEM with mapped infinite elements

In the finite element analysis, the infinite domain problems are solved in various ways, e.g., by a truncating of the domain as we used in our previous papers [12, 24], and now we have decided to use the so-called mapped infinite elements (MIE) which can be easily implemented. The MIE were originally pioneered by Bettess in [5] and later developed in [6, 23, 38, 39]. To derive our FEM numerical scheme for solving (11)–(13), we will follow the ideas presented in these works and we will combine them with the basic principles of FEM published in book by Reddy [29]. In this way, we will also naturally continue in our previous studies [21, 34].

3.1. Discretization of the computational domain

To use MIE, we divide the infinite computational domain Ω into two concentric parts, where the lower one, denoted by Ω_{FE}, is meshed with finite elements and the upper one, Ω_{MIE}, is meshed with one layer of infinite elements (Fig. 1 (a)). Since in our case $\partial\Omega$ is a triangulated Earth's surface, we have chosen triangular prisms, i.e., finite pentahedral elements with six nodes and five faces (Fig. 1 (b)), and corresponding mapped infinite pentahedral elements with nine nodes and five faces (Fig. 1 (c)). In this way, we divide the computational domain Ω into n_1, n_2, n_3 elements $\Omega^e, e = 1, \ldots, n_1 n_2 n_3$, in the latitudinal, longitudinal and vertical direction, respectively, and to specify the position of an element Ω^e we use indexes k, l, m, where $k = 1, \ldots, n_1$, $l = 1, \ldots, n_2$ and $m = 1, \ldots, n_3$.

3.2. Derivation of the weak formulation on the element

Let us consider an arbitrary element Ω^e from our finite element discretization with indeces $k = 1, \ldots, n_1$, $l = 1, \ldots, n_2$ and $m = 2, \ldots, n_3$. We multiply (11) by a weight function w and using Green's identity (we omit $(\mathbf{x})$ to simplify

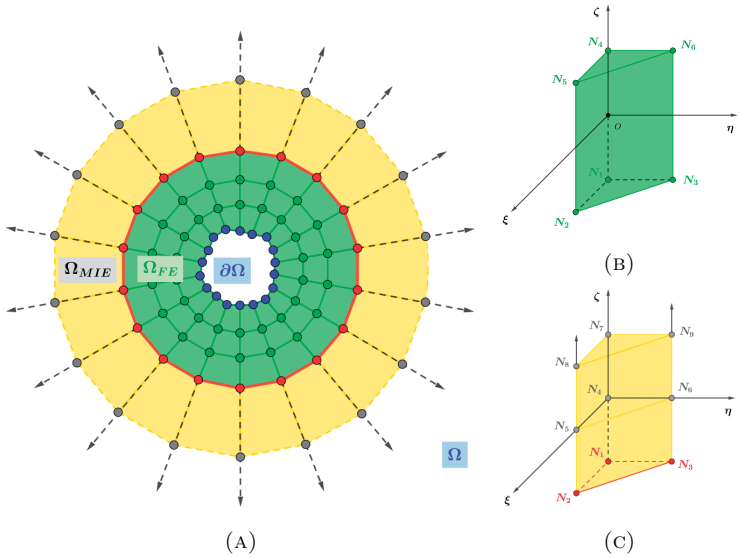

FIGURE 1. The meshed computational domain:
(a) Illustration of the computational domain Ω bounded by blue boundary $\partial\Omega$ and meshed with finite elements depicted by green, and one layer of mapped infinite elements depicted by yellow;
(b) The finite pentahedral elements with six nodes;
(c) The mapped infinite pentahedral elements with nine nodes. Isoparametric coordinates are within intervals $0 \leq \xi \leq 1$, $0 \leq \eta \leq 1$ and $-1 \leq \zeta \leq 1$.

the notation in the following equations) we obtain the weak formulation (WF) of (11) over an arbitrary above defined element Ω^e

$$\int_{\Omega^e} \nabla T \cdot \nabla w \, \mathrm{d}x\mathrm{d}y\mathrm{d}z = \int_{\partial\Omega^e} \nabla T \cdot \mathbf{n} \, w \, \mathrm{d}\sigma, \tag{15}$$

where $\mathbf{n}$ denotes the unit normal to $\partial\Omega^e$.

Due to the oblique derivative BC (12) prescribed on the bottom boundary Γ, we have to derive the WF for elements with indices $k = 1, \ldots, n_1$, $l = 1, \ldots, n_2$ and $m = 1$ separately. We use the ideas published in [20] or [24]. We split the oblique vector $\mathbf{v}$ into one normal, $\mathbf{n}$, and two tangential, $\mathbf{t}_1$, $\mathbf{t}_2$, components

$$\mathbf{v} = c_1\mathbf{n} + c_2\mathbf{t}_1 + c_3\mathbf{t}_2, \tag{16}$$

and we insert (16) into (12)

$$\nabla T \cdot \mathbf{v} = c_1 \nabla T \cdot \mathbf{n} + c_2 \nabla T \cdot \mathbf{t}_1 + c_3 \nabla T \cdot \mathbf{t}_2 = \alpha. \tag{17}$$

From (17) we express the normal derivative

$$\nabla T\cdot \mathbf{n} = \frac{\alpha}{c_1} - \frac{c_2}{c_1}\frac{\partial T}{\partial \mathbf{t}_1} - \frac{c_3}{c_1}\frac{\partial T}{\partial \mathbf{t}_2}, \tag{18}$$

where we assume that $c_1 \neq 0$, and we insert (18))to (15) to get

$$\int\limits_{\Omega^e} \nabla T\cdot\nabla w\,\mathrm{d}x\mathrm{d}y\mathrm{d}z = \int\limits_{\Gamma^e}\left(\frac{\alpha}{c_1} - \frac{c_2}{c_1}\frac{\partial T}{\partial \mathbf{t}_1} - \frac{c_3}{c_1}\frac{\partial T}{\partial \mathbf{t}_2}\right) w\,\mathrm{d}\sigma + \int\limits_{\partial\Omega^e\setminus\Gamma^e} \nabla T\cdot\mathbf{n}\,w\,\mathrm{d}\sigma. \tag{19}$$

After some rearrangement, we obtain the WF for elements with indices $k = 1, \ldots, n_1$, $l = 1, \ldots, n_2$ and $m = 1$

$$\int\limits_{\Omega^e} \nabla T\cdot\nabla w\,\mathrm{d}x\mathrm{d}y\mathrm{d}z + \frac{c_2}{c_1}\int\limits_{\Gamma^e}\frac{\partial T}{\partial \mathbf{t}_1}\,w\,\mathrm{d}\sigma + \frac{c_3}{c_1}\int\limits_{\Gamma^e}\frac{\partial T}{\partial \mathbf{t}_2}\,w\,\mathrm{d}\sigma = \int\limits_{\Gamma^e}\frac{\alpha}{c_1}\,w\,\mathrm{d}\sigma + \int\limits_{\partial\Omega^e\setminus\Gamma^e}\nabla T\cdot\mathbf{n}\,w\,\mathrm{d}\sigma, \tag{20}$$

where $\mathbf{n}$ is the normal vector and $\mathbf{t}_1$, $\mathbf{t}_2$ are tangent vectors to $\Gamma^e \subset \partial\Omega^e \subset R^3$, where Γ^e denotes the bottom boundary of an element Ω^e.

3.3. Derivation of equations over an element

For a pentahedral element Ω^e with indexes $k = 1, \ldots, n_1$, $l = 1, \ldots, n_2$ and $m = 2, \ldots, n_3 - 1$ with six nodes we can write

$$T \approx T^e = \sum_{j=1}^{6} T_j^e \psi_j, \tag{21}$$

i.e., we approximate the unknown value T as T^e using a linear combination of basis functions ψ_j with coefficients T_j^e, $j = 1, \ldots, 6$. We substitute (21)) into the WF (15) and consider ψ_i for weight function w. We obtain the ith equation in the form

$$\begin{aligned}\sum_{j=1}^{6} T_j^e \int\limits_{\Omega^e}\left(\frac{\partial\psi_j}{\partial x}\frac{\partial\psi_i}{\partial x} + \frac{\partial\psi_j}{\partial y}\frac{\partial\psi_i}{\partial y} + \frac{\partial\psi_j}{\partial z}\frac{\partial\psi_i}{\partial z}\right)\mathrm{d}x\mathrm{d}y\mathrm{d}z \\ = \sum_{j=1}^{6}\int\limits_{\partial\Omega^e} q_n\,\psi_i\,\mathrm{d}x\mathrm{d}y,\end{aligned} \tag{22}$$

where $q_n = \nabla T\cdot\mathbf{n}$ denotes the projection of the vector ∇T along the unit normal $\mathbf{n}$.

For the row of elements Ω^e given by indices $k = 1, \ldots, n_1$, $l = 1, \ldots, n_2$ and $m = 1$, we follow the same way and after inserting (21) into (20) and considering $w = \psi_i$, we obtain the ith equation in the form

$$\begin{aligned}
&\sum_{j=1}^{6} T_j^e \int\limits_{\Omega^e} \left(\frac{\partial \psi_j}{\partial x}\frac{\partial \psi_i}{\partial x} + \frac{\partial \psi_j}{\partial y}\frac{\partial \psi_i}{\partial y} + \frac{\partial \psi_j}{\partial z}\frac{\partial \psi_i}{\partial z} \right) \mathrm{d}x\mathrm{d}y\mathrm{d}z \\
&\quad + \sum_{j=1}^{3} T_j^e \left(\frac{c_2}{c_1} \int\limits_{\Gamma^e} \frac{\partial \psi_j}{\partial \mathbf{t}_1} \psi_i \, \mathrm{d}x\mathrm{d}y + \frac{c_3}{c_1} \int\limits_{\Gamma^e} \frac{\partial \psi_j}{\partial \mathbf{t}_2} \psi_i \, \mathrm{d}x\mathrm{d}y \right) \\
&= \sum_{j=1}^{3} \int\limits_{\Gamma^e} \frac{\alpha_j}{c_1} \psi_i \, \mathrm{d}x\mathrm{d}y + \sum_{j=1}^{6} \int\limits_{\partial\Omega^e \setminus \Gamma^e} q_n \, \psi_i \, \mathrm{d}x\mathrm{d}y,
\end{aligned} \tag{23}$$

where index $j = 1, \ldots, 3$ refers to nodes of the element Ω^e that lie on the bottom boundary Γ of the computational domain Ω.

Finally, for the mapped infinite pentahedral element Ω^e given by indices $k = 1, \ldots, n_1$, $l = 1, \ldots, n_2$ and $m = n_3$ with nine nodes, see Fig. 1 (c), we can write

$$T \approx T^e = \sum_{j=1}^{9} T_j^e \psi_j(x, y, z). \tag{24}$$

We substitute (24) for elements Ω^e with indexes $k = 1, \ldots, n_1$, $l = 1, \ldots, n_2$ and $m = n_3$ into (15), consider ψ_i for weight function w and we obtain the ith equation in the form

$$\begin{aligned}
&\sum_{j=1}^{9} T_j^e \int\limits_{\Omega^e} \frac{\partial \psi_j}{\partial x}\frac{\partial \psi_i}{\partial x} + \frac{\partial \psi_j}{\partial y}\frac{\partial \psi_i}{\partial y} + \frac{\partial \psi_j}{\partial z}\frac{\partial \psi_i}{\partial z} \, \mathrm{d}x\mathrm{d}y\mathrm{d}z \\
&= \sum_{j=1}^{9} \int\limits_{\partial\Omega^e} q_n \, \psi_i \, \mathrm{d}x\mathrm{d}y,
\end{aligned} \tag{25}$$

where $q_n = \nabla T \cdot \mathbf{n}$ again denotes the projection of the vector ∇T along the unit normal $\mathbf{n}$.

3.3.1. Shape and mapped functions

The basis function ψ_i is the piecewise quadratic function and it is uniquely determined by choosing value 1 at N_i and 0 at every $N_j, i \neq j$, cf. [8]. In our approach, we will work with isoparametric coordinates ξ, η, ζ in local coordinate

system, so we transform (21)) and (24) to, respectively,

$$T^e = \sum_{j=1}^{6} T_j^e \psi_j(\xi, \eta, \zeta), \tag{26}$$

$$T^e = \sum_{j=1}^{9} T_j^e \psi_j(\xi, \eta, \zeta), \tag{27}$$

where the transformation between local coordinates ξ, η, ζ and global coordinates x, y, z is given by

$$\begin{bmatrix} \frac{\partial \psi_i}{\partial \xi} \\ \frac{\partial \psi_i}{\partial \eta} \\ \frac{\partial \psi_i}{\partial \zeta} \end{bmatrix} = \begin{bmatrix} \frac{\partial x}{\partial \xi} & \frac{\partial y}{\partial \xi} & \frac{\partial z}{\partial \xi} \\ \frac{\partial x}{\partial \eta} & \frac{\partial y}{\partial \eta} & \frac{\partial z}{\partial \eta} \\ \frac{\partial x}{\partial \zeta} & \frac{\partial y}{\partial \zeta} & \frac{\partial z}{\partial \zeta} \end{bmatrix} \begin{bmatrix} \frac{\partial \psi_i}{\partial x} \\ \frac{\partial \psi_i}{\partial y} \\ \frac{\partial \psi_i}{\partial z} \end{bmatrix}. \tag{28}$$

Then the shape functions $\psi_i(\xi, \eta, \zeta)$ for finite pentahedral element with six nodes (see Fig.1 (b)) in the local coordinate system are defined in Tab. 1.

TABLE 1. The shape functions $\psi_i(\xi, \eta, \zeta)$ for the finite pentahedral element with six nodes N_i defined by isoparametric coordinates ξ, η and ζ.

N_i	ξ	η	ζ	Shape functions $\psi_i(\xi, \eta, \zeta)$
N_1	0	0	-1	$(1-\xi-\eta)(1-\zeta)/2$
N_2	1	0	-1	$\xi(1-\zeta)/2$
N_3	0	1	-1	$\eta(1-\zeta)/2$
N_4	0	0	1	$(1-\xi-\eta)(1+\zeta)/2$
N_5	1	0	1	$\xi(1+\zeta)/2$
N_6	0	1	1	$\eta(1+\zeta)/2$

In the fixed GBVP (11)–(13), the computational domain Ω tends to infinity only in the vertical direction. So let us suppose the element Ω^e which extends from node N_1 with coordinate x_1 through N_2 with coordinate x_2 to the point N_3 at infinity, see Fig 2. Then this element is mapped onto the parent element defined in the local coordinate system in the range $-1 < \zeta < 1$ using formula

$$x(\zeta) = M_1(\zeta)x_1 + M_2(\zeta)x_2, \tag{29}$$

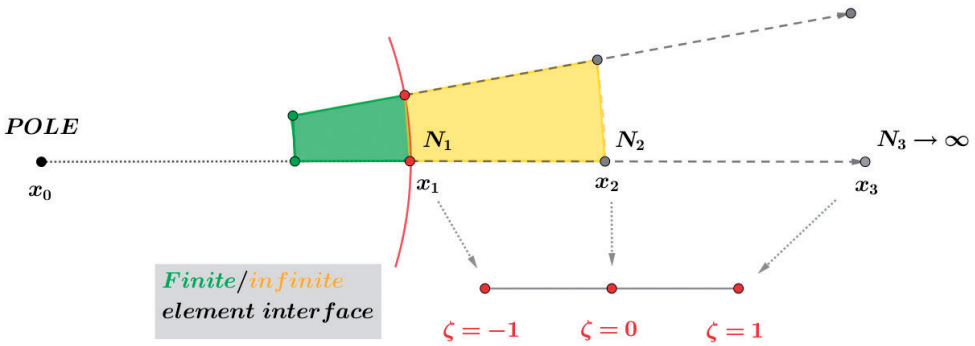

FIGURE 2. Illustration of MIE tending to infinity in the vertical direction Ω^e.

where

$$M_1(\zeta) = \frac{-2\zeta}{1-\zeta}, \tag{30}$$

$$M_2(\zeta) = \frac{1+\zeta}{1-\zeta}. \tag{31}$$

It is obvious from (29)–(31) that $\zeta = -1, 0, 1$ correspond to the global positions of x_1, x_2, ∞, respectively. Then for infinite pentahedral element with nine nodes N_i, see Fig. 1 (c), we obtain the mapping functions $M_i(\xi, \eta, \zeta)$ by multiplying (30)–(31) with the shape functions $\psi_i(\xi, \eta)$ for linear triangular element, where directions ξ and η are finite, i.e.,

$$\psi_1(\xi, \eta) = 1 - \xi - \eta, \quad \psi_2(\xi, \eta) = \xi \quad \text{and} \quad \psi_3(\xi, \eta) = \eta.$$

These mapping functions $M_i(\xi, \eta, \zeta)$ can be seen in Tab. (2).

Now we can write (22), (23) and (25) in a compact matrix form

$$\mathbf{K}^e \, \mathbf{T}^e = \mathbf{Q}^e, \tag{32}$$

where $\mathbf{K}^e = [K_{ij}]$ stands for an element stiffness matrix, $\mathbf{T}^e = (T_1, \ldots, T_6)$ is a column vector of unknowns and $\mathbf{Q}^e$ denotes the right-hand side vector.

To evaluate element matrices and vectors we proceed as follows. We choose one basis function ψ_i per vertex N_i^e and we differentiate the basis functions with respect to a position of each node. To calculate two integrals over a boundary Γ in (23) which include a tangential derivative, we approximate derivatives in tangential direction like in the finite difference method, i.e., using values of basis functions at nodes N_i, see Fig. 3, of element e we have

TABLE 2. The mapping functions $M_i(\xi,\eta,\zeta)$ for the infinite pentahedral element with nine nodes N_i which extends to infinity in the vertical direction. Values ξ, η and ζ denote isoparametric coordinates of nodes.

N_i	ξ	η	ζ	Mapping functions $M_i(\xi,\eta,\zeta)$
N_1	0	0	-1	$(1-\xi-\eta)\,(-2\zeta)/(1-\zeta)$
N_2	1	0	-1	$\xi(-2\zeta)/(1-\zeta)$
N_3	0	1	-1	$\eta(-2\zeta)/(1-\zeta)$
N_4	0	0	0	$(1-\xi-\eta)\,(1+\zeta)/(1-\zeta)$
N_5	1	0	0	$\xi(1+\zeta)/(1-\zeta)$
N_6	0	1	0	$\eta(1+\zeta)/(1-\zeta)$
N_7	0	0	1	-
N_8	1	0	1	-
N_9	0	1	1	-

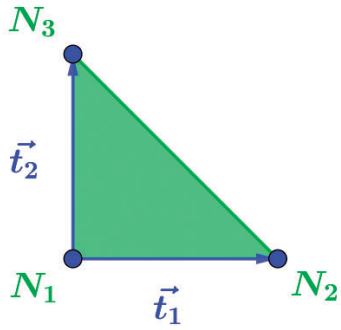

FIGURE 3. Illustration of tangent vectors used for approximating the tangential derivatives.

$$\frac{\partial \psi_j^{(e)}}{\partial \mathbf{t}_1} \approx \frac{\psi_j^{(e)}(N_2) - \psi_j^{(e)}(N_1)}{d(N_1,N_2)}, \tag{33}$$

$$\frac{\partial \psi_j^{(e)}}{\partial \mathbf{t}_2} \approx \frac{\psi_j^{(e)}(N_3) - \psi_j^{(e)}(N_1)}{d(N_1,N_3)}, \tag{34}$$

where d denotes the distance between two neighbouring nodes. The same idea of approximating derivatives, however for hexahedral elements, has been presented in [24].

3.4. Assembly of element equations

Finally, we assemble all element equations using two principles, see Reddy [29]:

(i) continuity of primary variables at the interelement nodes. It means that nodal values T_j^e and T_j^{e+1} of two adjacent elements Ω^e and Ω^{e+1} at the connecting nodes have to be the same.

(ii) balance of secondary variables in a weighted-integral sense.

In this manner, we obtain the global linear system of equations with a column vector of unknown global nodal values $\mathbf{T}$,

$$\mathbf{KT} = \mathbf{Q}, \tag{35}$$

where the matrix $\mathbf{K}$ is sparse, since most of its entries are zero, which is a basic feature of the FEM, see [8, 29], and positive definite, and $\mathbf{Q}$ is the column vector whose entries are zero except for nodes with the prescribed oblique derivative BC (12).

4. Numerical experiments

We have performed three numerical experiments. The first experiment has dealt with the modelling disturbing potential obtained as a difference between gravitational potentials generated by two homogeneous spheres with mutually displaced origins. The aim of this experiment was to test a behaviour of the proposed approach on the example where the exact solution is known.

In the second experiment, the reconstruction of Earth Gravitational Model 2008 (EGM2008) [28] on the discretized Earth's surface has been done and studied.

The last experiment has dealt with detailed global gravity field modelling using the DTU21GRAV data [1]. This database provides the high-resolution altimetry-derived gravity data over ocean/seas augmented by the EGM2008--based gravity data over lands improved by a detailed terrain effect.

4.1. Experiment with the homogeneous spheres

The first experiment was theoretical, involving an artificial situation, just to study and test the behaviour of the proposed approach, and it was equivalent to the experiment published in [22]. In this simplified testing case, the disturbing field has been generated between two identical homogeneous spheres with the radius $R = 6378\,[\mathrm{km}]$ but with centers mutually shifted by $100\,[\mathrm{km}]$ in the z-direction, see Fig. 4.

The gravitational potential as the exact solution of (11) has been calculated as GM/r, where GM denotes the geocentric gravitational constant and r denotes the distance from the origin O or O^*, see Fig. 4. To obtain BC on the bottom boundary, the derivative of this exact solution in the form $-\mathrm{GM}/r^2$ has

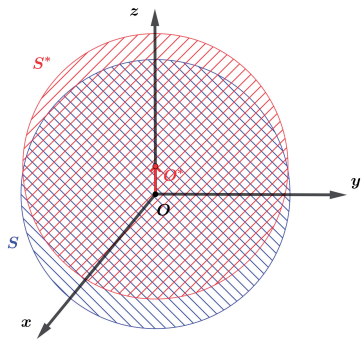

FIGURE 4. The illustration of the testing numerical experiment – – the disturbing potential is obtained between the gravitational potential generated by the sphere S representing the simplified Earth, and the gravitational potential generated by the sphere S^* representing the normal body.

been used. We have started (see Tab. 3) with the resolution $180 \times 90 \times 45$, where the numbers denote the number of nodes in longitudinal, latitudinal and radial direction, respectively. Afterwards, we have performed two successive refinements and in each refinement we have calculated four iterations. We can see that with the refinement, we have obtained the convergence of the method, and moreover, it is obvious that the second iteration of our solution is very close to the "Reference" value (see Tab. 3), so the following iterations bring only small improvement of the results. In this case, the "Reference" value is used to designate the values obtained with the exactly calculated vector $\mathbf{v(x)}$ (see e.g. (12)), so this value includes only the discretization error.

For a comparison, we have also performed the corresponding experiment, where we have solved the nonlinear satellite-fixed GBVP, see [22], by the FEM with the domain truncated at the altitude of 240 km. There the disturbing potential calculated as GM/r was prescribed. The size of the elements was chosen identical to the previous experiment. Statistics of residuals between the obtained solution and the disturbing potential directly calculated as GM/r can be seen in Tab. 4. It is obvious that again when the grid is refined, the standard deviation decreases by approximately 4 times. However, minimum and maximum values as well as the standard deviation of residuals are significantly lower in comparison to the values presented in the Tab. 3. It is an expected consequence of fixing the solution with the Dirichlet BC at the altitude of 240 km. It shows that if sufficiently accurate and reliable data are available at the boundary outside the Earth, it is reasonable to solve nonlinear satellite-fixed GBVP, but if such data are not available, solving the INFGBVP by FEM with MIE is an appropriate and useful alternative.

TABLE 3. Statistics of residuals between the numerical solution to the INFGBVP and the exact solution obtained as GM/r on the bottom boundary (units: $m^2 s^{-2}$). The "Reference" values are obtained with exactly calculated vector $\mathbf{v(x)}$, see (12).

No. of nodes	No. of it.	Min.	Max.	Mean	St. deviation
$180 \times 90 \times 45$	1	27.3510	60.4258	47.0674	9.5872
	2	-66.1024	67.5531	0.2961	44.3976
	3	-66.1023	67.5517	0.2953	44.3969
	4	-66.1023	67.5517	0.2953	44.3969
	Reference	-66.1033	67.5526	0.2953	44.3978
$360 \times 180 \times 90$	1	32.3182	59.6482	47.0545	8.9062
	2	-16.6631	17.6192	0.1483	11.1865
	3	-16.6633	17.6189	0.1479	11.1864
	4	-16.6632	17.6189	0.1480	11.1864
	Reference	-16.6634	17.6190	0.1480	11.1865
$720 \times 360 \times 180$	1	33.2430	59.5323	47.0267	8.8453
	2	-4.3218	5.5170	0.2273	2.9748
	3	-4.4008	5.4692	0.1257	2.9766
	4	-4.4008	5.4692	0.1257	2.9766
	Reference	-4.3944	5.2340	0.1134	2.9686

4.2. Global gravity field modelling with the EGM2008 as a reconstruction of the harmonic function

In case of the experiment with the EGM2008, the bottom boundary Γ has been the discretized Earth's surface created with SRTM30 PLUS data, see [4]. The height of Ω_{FE} has been 5000 [km]. The number of divisions has been $360 \times 180 \times 90$, $720 \times 360 \times 180$ and $1440 \times 720 \times 360$ corresponding to horizontal resolution $1\,\mathrm{deg} \times 1\,\mathrm{deg}$, $0.5\,\mathrm{deg} \times 0.5\,\mathrm{deg}$ and $0.25\,\mathrm{deg} \times 0.25\,\mathrm{deg}$, respectively. The input surface gravity disturbances as BC (12) have been generated from EGM2008 [28].

The disturbing potential solution for the finest grid, i.e., $1440 \times 720 \times 360$ is depicted in Fig. 5. Statistics of residuals on the Earth's surface between the obtained solution and the disturbing potential generated directly from EGM2008 for successive refinements can be found in Tab. 5. We can see an improvement

TABLE 4. Statistics of residuals between the FEM solution to the satellite-fixed GBVP [22] and the exact solution on Γ (units: $m^2 s^{-2}$). The "Reference" values are obtained with exactly calculated vector $\mathbf{v(x)}$, see (12).

No. of nodes	No. of it.	Min.	Max.	Mean	St. deviation
$180 \times 90 \times 5$	1	-1.7373	2.8744	1.3906	1.4734
	2	-2.5845	2.6150	0.0078	1.9819
	3	-2.5845	2.6149	0.0078	1.9819
	4	-2.5845	2.6149	0.0078	1.9819
	Reference	-2.5845	2.6149	0.0078	1.9819
$360 \times 180 \times 10$	1	-0.4422	2.7906	1.3932	1.0235
	2	-0.6346	0.6422	0.0019	0.4873
	3	-0.6346	0.6422	0.0019	0.4873
	4	-0.6346	0.6422	0.0019	0.4873
	Reference	-0.6346	0.6422	0.0019	0.4873
$720 \times 360 \times 20$	1	-0.1075	2.7838	1.3938	0.9852
	2	-0.1580	0.1599	0.00049	0.1213
	3	-0.1580	0.1599	0.00049	0.1213
	4	-0.1580	0.1599	0.00049	0.1213
	Reference	-0.1580	0.1599	0.00049	0.1213

of all statistical characteristics when refining the computational grid. The differences between the obtained solution and the disturbing potential generated from EGM2008 directly for the finest grid are depicted in Fig. 6. We can observe the biggest differences at the borders of the continents or significant terrain changes, which are the result of still coarse discretization, i.e., resolution $0.25\,\mathrm{deg} \times 0.25\,\mathrm{deg}$. The contribution of the first iteration in the disturbing potential solution is depicted in Fig. 7. As we have expected from our previous study [22], the iterative process changes the solution in areas with steep changes in the disturbing potential, although these changes, see Fig. 7, are very small.

For a comparison, we have performed the corresponding experiment with the corresponding resolution, see Tab. 6, where the computational domain was

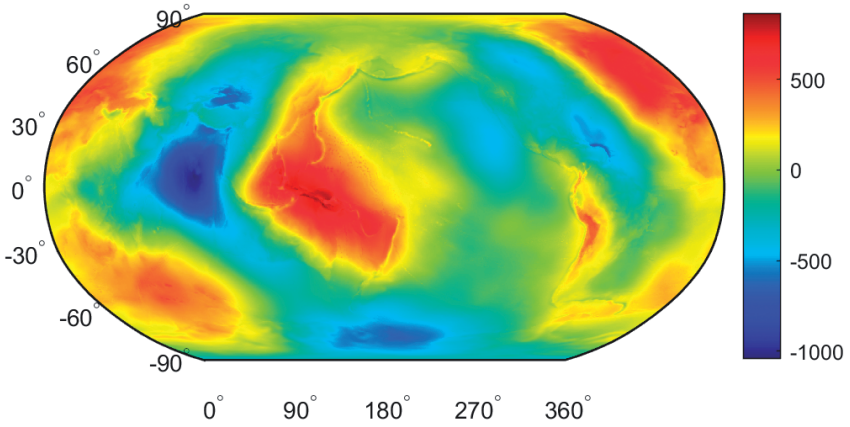

FIGURE 5. Global gravity field modelling with the EGM2008: The disturbing potential solution by solving INFGBVP in $1440 \times 720 \times 360$ grid (units: $m^2 s^{-2}$).

TABLE 5. Statistics of residuals between the FEM with MIE solution to the INFGBVP and the disturbing potential generated from EGM2008 directly on the bottom boundary (units: $m^2 s^{-2}$).

No. of nodes	No. of it.	Min.	Max.	Mean	St. deviation
$360 \times 180 \times 90$	1	-267.505	193.158	14.173	16.848
	2	-267.744	192.956	14.094	16.842
	3	-267.744	192.956	14.094	16.842
$720 \times 360 \times 180$	1	-109.916	88.818	2.382	6.787
	2	-110.014	88.650	2.317	6.784
	3	-110.014	88.650	2.317	6.784
$1440 \times 720 \times 360$	1	-37.716	55.803	0.570	2.054
	2	-37.892	55.691	0.516	2.050
	3	-37.892	55.691	0.516	2.050

truncated at the altitude 240 [km] and where we prescribed disturbing potential generated from EGM2008. Statistics of residuals on the Earth's surface between the obtained solution and the disturbing potential generated directly from EGM2008 for successive refinements can be found in Tab. 6. We notice that values of standard deviation are smaller in comparison to values presented in Tab. 5, but on the other hand, we can see that they converge to each other by refinement. The differences between the obtained solution and the disturbing potential generated from EGM2008 directly for the finest grid are depicted in Fig. 8.

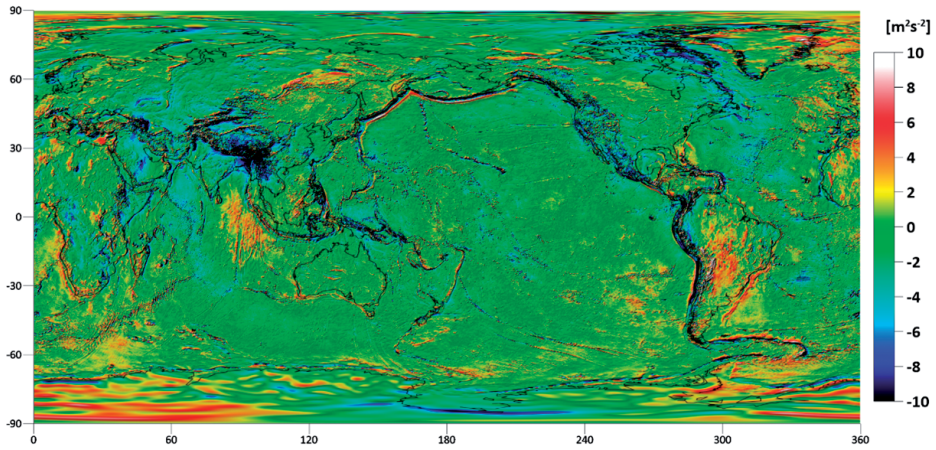

FIGURE 6. Global gravity field modelling with the EGM2008:
The differences between the INFGBVP solution by FEM with MIE and disturbing potential generated from EGM2008 directly.

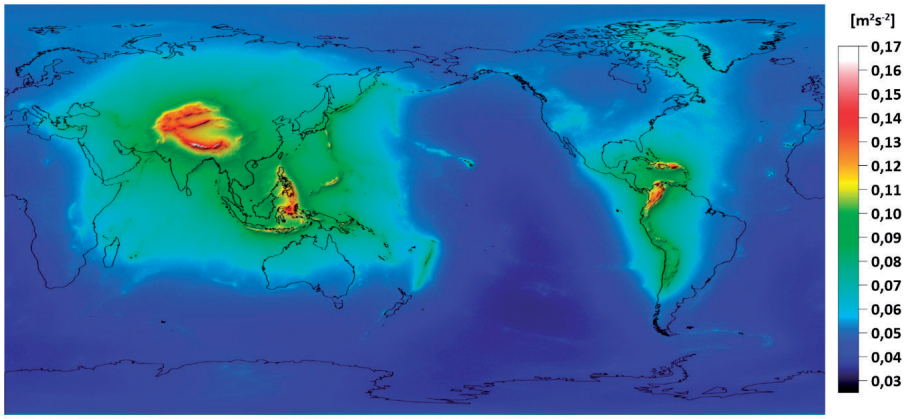

FIGURE 7. Global gravity field modelling with the EGM2008:
The contribution of the first iteration in the disturbing potential solution when solving the INFGBVP by FEM with MIE.

When comparing the Fig. 6 and Fig. 8, in case of FEM with MIE we notice higher differences in the Himalayan region, part of Indonesia and selected areas of Central America, but, on the other hand, in the area of Australia and

New Zealand these differences are smaller. The contribution of the first iteration in the disturbing potential solution is depicted in Fig. 9. We can observe a difference in comparison to Fig. 7 which is a consequence of different concept in taking into account the regularity of the disturbing potential. This proves our assumption that if we have the correct values of the Dirichlet BC in the infinite computational domain, it is appropriate to truncate the computational domain and take them into account. However, if we do not have such data, then the use of MIE is a suitable approach, since by refining the computational grid, the solution becomes more precise and moreover one can improve the solution in the areas with high values of deflection of vertical when taken into account the nonlinear BC.

TABLE 6. Statistics of residuals between the FEM solution to the satellite-fixed GBVP [22] and the disturbing potential generated from EGM2008 directly on the bottom boundary (units: $m^2 s^{-2}$).

No. of nodes	No. of it.	Min.	Max.	Mean	St. deviation
$360 \times 180 \times 10$	1	-284.617	157.059	0.538	13.132
	2	-284.768	156.981	0.536	13.132
	3	-284.768	156.981	0.536	13.132
$720 \times 360 \times 20$	1	-106.447	73.866	0.011	5.127
	2	-106.483	73.826	0.008	5.127
	3	-106.483	73.826	0.008	5.127
$1440 \times 720 \times 40$	1	-40.293	45.928	0.006	1.648
	2	-40.376	45.917	0.004	1.648
	3	-40.376	45.917	0.004	1.648

4.3. Global gravity field modelling with DTU21GRAV data

In the last experiment, the bottom boundary Γ has been again the discretized topography created with SRTM30 PLUS data, see Becker et al. [4]. The height of Ω_{FE} has been 5000 [km] and the number of divisions has been $2880 \times 1440 \times 720$ corresponding to horizontal resolution 0.125 deg $\times$0.125 deg, respectively. The input surface gravity disturbances, see Fig. 10, as BC (12) applied on Γ have been generated from the DTU21GRAV data [1]. The disturbing potential solution is depicted in Fig. 11. The contribution of the iterative process in the disturbing potential solution is depicted in Fig. 12. We can observe that the values of differences have the similar behaviour in comparison to Fig. 7, namely the values and their location, which is related to areas with the high values of deflection of vertical.

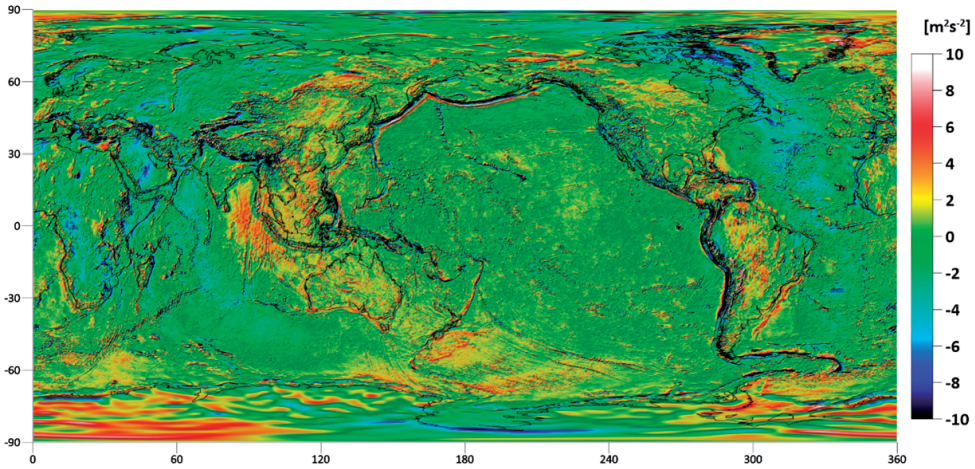

FIGURE 8. Global gravity field modelling with the EGM2008:
The differences between the nonlinear satellite-fixed GBVP solution by FEM and disturbing potential generated from EGM2008 directly.

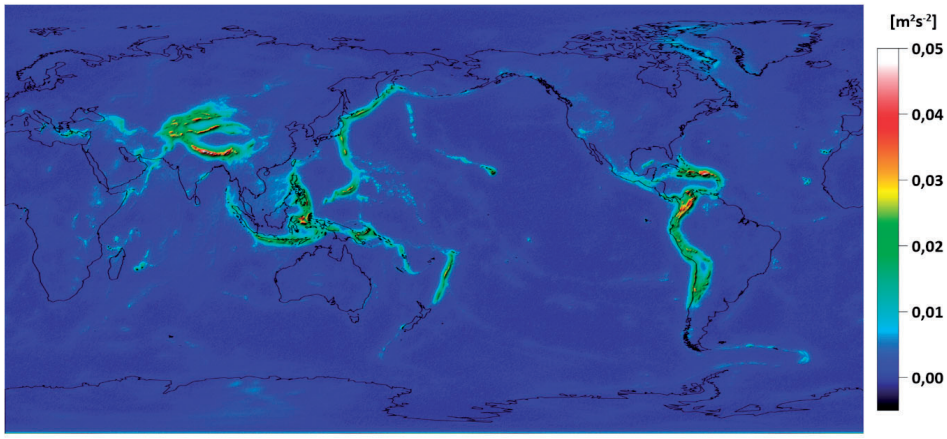

FIGURE 9. Global gravity field modelling with the EGM2008:
The contribution of the first iteration in the disturbing potential solution when solving the nonlinear satellite-fixed GBVP by FEM.

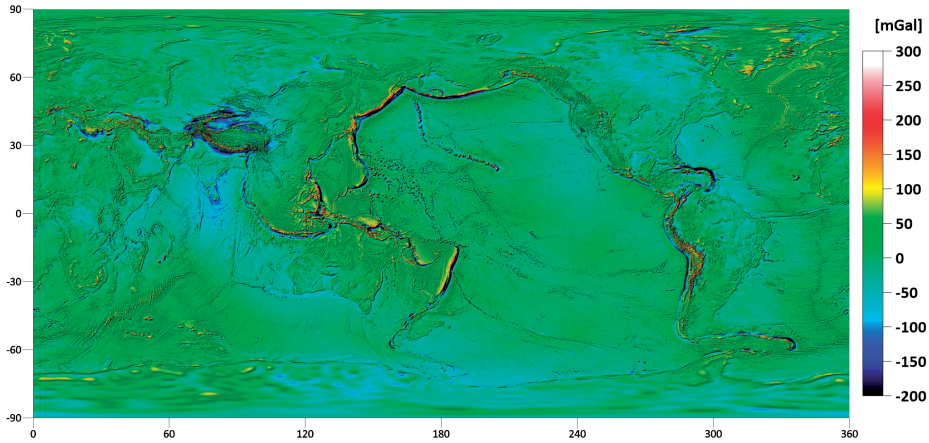

FIGURE 10. Global gravity field modelling with DTU21GRAV data: The surface gravity disturbances.

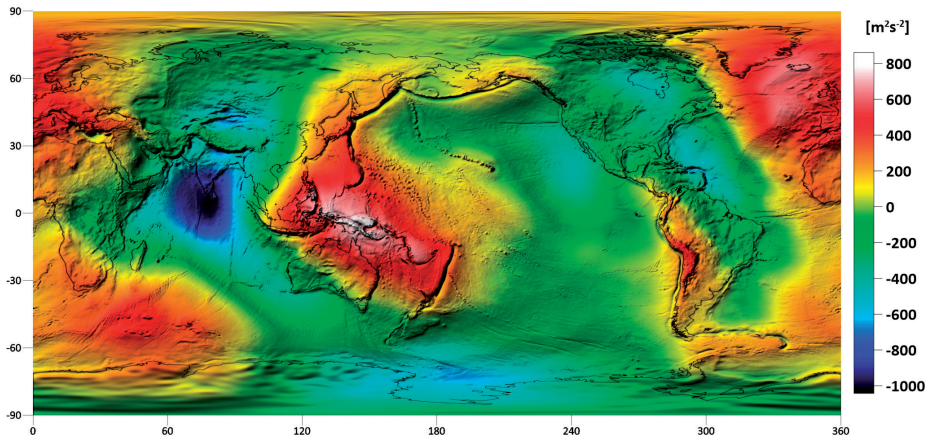

FIGURE 11. Global gravity field modelling with DTU21GRAV data: The disturbing potential solution after the first iteration by the FEM with MIE.

5. Conclusion and summary

The presented paper is a natural continuation and concluding study of our previous works focused on solving the fixed geodetic boundary value problems by the finite element method. In this paper, we have proposed, derived and implemented a numerical approach for solving the original infinite nonlinear

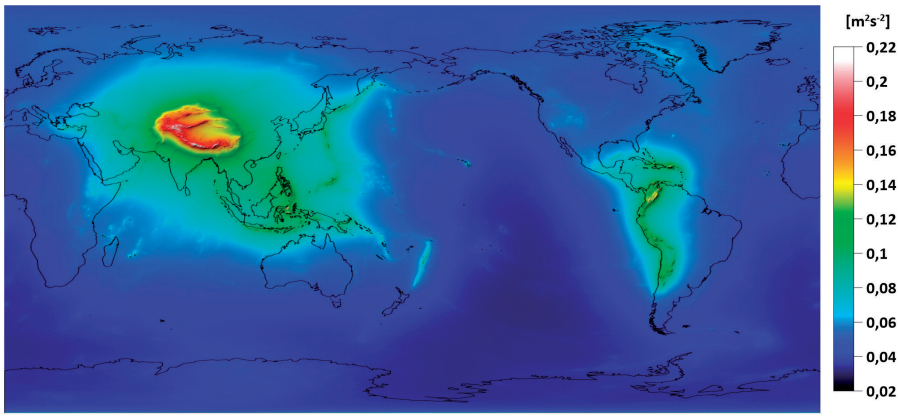

FIGURE 12. Global gravity field modelling with DTU21GRAV data: The differences between the first solution and the solution obtained after the last iteration.

fixed geodetic boundary value problem. This approach was based on the iterative procedure, which has led to the solution of the oblique derivative fixed geodetic boundary value problem by the finite element method, while to take into account the regularity of the disturbing potential at infinity, we have employed the mapped infinite elements. An advantage of using this approach for solving such BVP is that numerical solutions can be obtained on the discretized real Earth's surface considering its topography. This can be challenging in high-mountainous areas where a contribution of the nonlinearity is expected to be significant. The validity of this approach has been tested by one modelling numerical experiment and a numerical study focused on a reconstruction of the harmonic function (EGM2008) above the discretized Earth's topography was performed. In these experiments we have compared the obtained solutions with the solutions by the FEM with the truncated finite computational domain and prescribed disturbing potential. Results have showed the advantages of the truncation of computational domain by adding the artificial boundary with prescribed correct BC, as well as the fact that in cases when only the surface gravity disturbances are available, a solution by FEM with MIE is, under certain conditions, e.g., sufficiently fine grid, an appropriate and comparable alternative. This finding can be applied also to other BVPs where semi-infinite domain is of interest, but no Dirichlet BC are available. Finally, we have performed one more detailed experiment with DTU21GRAV data, where we have shown that the iterative process can improve the solution in areas with the steep changes in the disturbing potential, that two iterations are sufficient for this improvement.

Acknowledgements. We would like to thank the support given by Grants APVV-23-0186 and VEGA 1/0690/24 as well as an unknown erudite reviewer for a very precise reading of the paper and many stimulating comments that significantly improved the paper.

`Author Contribution Statement.`

Marek Macák developed the theory and performed the numerical experiments. Zuzana Minarechová contributed to develop the theory and wrote the manuscript. Róbert Čunderlík and Karol Mikula devised the project. All authors discussed the results and contributed to the final manuscript.

`Data Availability Statement.`

All datasets generated and/or analysed within the experiments are available from the corresponding author.

`Conflict of Interests/Competing Interests.`

All authors declare that they have no conflicts of interest.

REFERENCES

[1] ANDERSEN, O. B.—ABULAITIJIANG, A.—ZHANG, S.—ROSE, S. K.: *A new high resolution Mean Sea Surface (DTU21MSS) for improved sea level monitoring*, In: Proceedings of the EGU General Assembly (EGU21-16084), Vienna, Austria, April 19–30, 2021.

[2] BACKUS, G. E.: *Application of a non-linear boundary-value problem for Laplace's equation to gravity and geomagnetic intensity surveys*, Quart. J. Mech. Appl. Math. **2** (1968), 195–221.

[3] BARTHELMES, F.: *Definition of Functionals and of the Geopotential and Their Calculation From Spherical Harmonic Models Deutsches GeoForschungsZentrum GFZ*. Scientific Technical Report STR09/02, Potsdam, Germany, 2013.

[4] BECKER, J. J.—SANDWELL, D. T.—SMITH, W. H. F.—BRAUD, J.— BINDER, B.—DEPNER, J.—FABRE, D.—FACTOR, J.—INGALLS, S.— KIM, S. H.—LADNER, R.— MARKS, K.—NELSON, S.—PHARAOH, A.—TRIMMER, R.—ROSENBERG, J.—VON WALLACE, G.—WEATHERALL, P.: *Global bathymetry and elevation data at 30 arc seconds resolution: SRTM30 PLUS*, Marine Geodesy, **32** (2009), no. 4, 355–371, https://doi.org/10.1080/01490410903297766.

[5] BETTESS, P.: *Infinite elements*, Internat. J. Numer. Methods Engnr. **11** (1977), no. 1, 53–64.

[6] BETTESS, P.: *More on infinite elements*, Internat. J. Numer. Methods Engnr. **15** (1983), no. 11, 1613–1626.

[7] BJERHAMMAR, A.—SVENSSON, L.: *On the geodetic boundary value problem for a fixed boundary surface—A satellite approach*, Bulletin Géodésique **57** (1983), no. 1–4, 382–393.

[8] BRENNER, S. C.—SCOTT, L. R.: *The Mathematical Theory of Finite Element Methods*. 2nd ed. Springer-Verlag, Berlin, 2002.

[9] CARRIÓN SÁNCHEZ, J. L.—DE FREITAS, S.—BARZAGHI, R.: *Offset evaluation of the ecuadorian vertical datum related to the IHRS*, Bulletin of Geodetic Sciences **24** (2018), no. 4, 503–525, doi: 10.1590/s1982-21702018000400031.

[10] DÍAZ, G.—DÍAZ, J. I.—OTERO, J.: *On an oblique boundary value problem related to the Backus problem in geodesy*, Nonlinear Anal. Real World Appl. **7** (2006), no. 2, 147–166.

[11] DÍAZ, G.—DÍAZ, J. I.—OTERO, J.: *Construction of the maximal solution of Backus' problem in geodesy and geomagnetism*, Stud. Geophys. Geod. **55** (2011), no. 3, 415–440.

[12] FAŠKOVÁ, Z.—ČUNDERLÍK, R.—MIKULA, K.: *Finite element method for solving geodetic boundary value problems*, J. Geodesy **84** (2010), no. 2, 135-–144.

[13] HECK, B.: *On the non-linear geodetic boundary value problem for a fixed boundary surface*, Bull. Geodésy **63** (1989), no. 1, 57–67.

[14] HECK, B.—SEITZ, K.: *Effects of Non-Linearity in the Geodetic Boundary Value Problems*. German Geodetic Kommission (DGK), Series A, No. 109, Munchen, Germany, 1993.

[15] HOFMANN-WELLENHOF, B.—MORITZ, H.: *Physical Geodesy*. 2nd ed. Springer-Verlag, Vienna, 2006, https://doi.org/10.1007/978-3-211-33545-1

[16] HOTINE, M.: *Mathematical Geodesy*. ESSA Monograph Vol. 2, US Dept. of Commerce, Washington 1969.

[17] JEKELI, C.: *A numerical study of the divergence of spherical harmonic series of the gravity and height anomalies at the Earth's surface*, Bull. Géodésique, **57** (1983), no. 1–4, 10–28, doi: 10.1007/BF02520909.

[18] KOCH, K. R.—POPE, A. J.: *Uniqueness and existence for the geodetic boundary value problem using the known surface of the earth*, Bulletin Géodésique, **46** (1972), 467–476.

[19] MACÁK, M.—MIKULA, K.—MINARECHOVÁ, Z.—ČUNDERLÍK, R.: *On an iterative approach to solving the nonlinear satellite-fixed geodetic boundary-value problem*, In: IAG Symp **142** (2016), pp. 185–192.

[20] MACÁK, M.—MINARECHOVÁ, Z.—ČUNDERLÍK, R.—MIKULA, K.: *The finite element method as a tool to solve the oblique derivative boundary value problem in geodesy*, Tatra Mt. Math. Publ. **75** (2020), no. 1, 63–80.

[21] MACÁK, M.—MINARECHOVÁ, Z.—TOMEK, L.— ČUNDERLÍK, R.—MIKULA K.: *Solving the fixed gravimetric boundary value problem by the finite element method using mapped infinite elements*, Computational Geosciences, **27** (2023), 649–662.

[22] MACÁK, M.—MINARECHOVÁ, Z.—ČUNDERLÍK, R.—MIKULA, K.: *A gravity field modelling in mountainous areas by solving the nonlinear satellite-fixed geodetic boundary value problem with the finite element method*, Acta Geodaetica et Geophysica, **58** (2023), 305–320.

[23] MARQUES, J. M. M. C.—OWEN, D. R. J.: *Infinite elements in quasi-static materially nonlinear problems*, Computers & Structures, **18** (1984), no. 4, 739–751.

[24] MINARECHOVÁ, Z.—MACÁK, M.—ČUNDERLÍK, R.—MIKULA, K.: *On the finite element method for solving the oblique derivative boundary value problems and its application in local gravity field modelling*, J. Geodesy, **95** (2021), art. no. 70.

[25] MOLODENSKII, M. S.—EREMEEV, V. F.—YURKINA, M. I.: *Methods for the Study of the External Gravitational Field and Figure of the Earth*. TRUDY Ts NIIGAiK, Vol. 131, Geodezizdat, Moscow, 1960.

[26] MORITZ, H.: *The Figure of the Earth: Theoretical Geodesy and the Earth's Interior*. Wichmann, Karlsruhe, Germany, 1990.

[27] MORITZ, H.: *Classical physical geodesy*. In: (W. Freeden, Z. M. Nashed, T. Sonar, eds.), Handbook of Geomathematics, Springer-Verlag, Berlin, Germany, 2010, pp. 127–158.

[28] PAVLIS, N.K.—HOLMES, S.A.—KENYON, S.C.—FACTOR, J.K.: *The development and evaluation of the Earth Gravitational Model 2008 (EGM2008)*, Journal of Geophysical Research **117** (2012), Issue B4; https://doi.org/10.1029/2011JB008916

[29] REDDY, J. N.: *An Introduction to the Finite Element Method*. 3rd ed. McGraw-Hill Education, New York, 2006.

[30] SACERDOTE, F.—SANSÓ, F.: *On the analysis of the fixed-boundary gravimetric boundary-value problem*. In: (F. Sacerdote, F. Sansó, eds.), Proceedings of the 2nd Hotine-Marussi Symposium on Mathematical Geodesy, Pisa, Politecnico di Milano, 1989, pp. 507–516.

[31] SETHIAN, J. A.: *Fast Marching Methods*. In: (B. Engquist, ed.) Encyclopedia of Applied and Computational Mathematics, Springer-Verlag, Berlin, Heidelberg, 2015.

[32] SJÖBERG, L. E.: *On the Errors of Spherical Harmonic Developments of Gravity at the Surface of the Earth*. Report No. 257, Department of Geodetic Science, The Ohio State University, Columbus, OH, USA, 1977.

[33] STOKES, G. G.: *On the variation of gravity on the surface of the Earth*, Trans. Cambr. Phil. Soc. **8** (1849), 672–695.

[34] 34 ŠPRLÁK, M.—FAŠKOVÁ, Z.—MIKULA, K.: *On the application of the coupled finite-infinite element method to the geodetic boundary value problem*, Studia Geophysica et Geodaetica **55** (2011), 479–487.

[35] ŠPRLÁK, M.—HAN, S.-C.—FEATHERSTONE, W.: *Forward modelling of global gravity fields with 3D density structures and an application to the high-resolution (2km) gravity fields of the Moon*, **92** (2018), no. 8, 847–862, doi: 10.1007/s00190-017-1098-7.

[36] ŠPRLÁK, M.—HAN, S.-C.—FEATHERSTONE, W.: *Spheroidal forward modelling of the gravitational fields of 1 Ceres and the Moon*, Icarus **335**, art. no. 113412, `https://doi.org/10.1016/j.icarus.2019.113412`

[37] ŠPRLÁK, M.—HAN, S.-C.: *On the use of spherical harmonic series inside the minimum Brillouin sphere: Theoretical review and evaluation by GRAIL and LOLA satellite data*, Earth-Science Reviews **222**, 2021, art. no. 103739, `https://doi.org/10.1016/j.earscirev.2021.103739`

[38] ZIENKIEWICZ, O. C.—EMSON, C.—BETTESS, P.: *A novel boundary infinite element*, Internat. J. Numer. Meth. Engnr. **19** (1983), 340–393.

[39] ZIENKIEWICZ, O. C.—BANDO, K.—BETTESS, P.—EMSON, C.—CHIAM, T. C.: *Mapped infinite elements for exterior wave problems*, Internat. J. Numer. Meth. Engnr. **21** (1985), 1229–1251.

Received September 11, 2024
Revised November 25, 2024
Accepted December 2, 2024
Publ. online September 30, 2025

Faculty of Civil Engineering
Slovak University of Technology
Department of Mathematics and Descriptive Geometry
Radlinského 11
810 05 Bratislava
SLOVAKIA

E-mail: marek.macak@stuba.sk
zuzana.minarechova@stuba.sk
robert.cunderlik@stuba.sk
karol.mikula@stuba.sk